Integrating the *IMSA* with Bayesian Compressive Sensing for Solving Inverse Scattering Problems

N. Anselmi, L. Poli, G. Oliveri, and A. Massa

Abstract

A novel microwave imaging technique is proposed in this work for solving 2D transverse magnetic inverse scattering problems under the first order Born approximation. The developed strategy exploits the well-known regularization capabilities of Bayesian compressive sensing (*BCS*) and the progressively acquired information through a multi-resolution iterative approach. Towards this end, a customized relevance vector machine (*RVM*) solver is implemented to iteratively improve the *BCS* solution accuracy within the identified region of interest (*RoI*). Selected numerical results are shown to verify the effectiveness of the proposed methodology.

1 Numerical Results

1.1 Inhomogeneous Square Object, $\ell = 1.5\lambda$

Test Case Description

Direct solver:

- Side of the investigation domain: $L = 6.0\lambda$
- Cubic domain divided in $\sqrt{D} \times \sqrt{D}$ cells
- Number of cells for the direct solver: $D = 1600$ (discretization $= \lambda/10$)

Investigation domain:

- Cubic domain divided in $\sqrt{N} \times \sqrt{N}$ cells
- Number of cells for the inversion:
  - First Step IMSA: $N^{(1)} = 100$ (discretization $= \lambda/10$)
  - Following Steps IMSA: $N^{(i)}$ not fixed, defined according to the estimated RoI $\mathcal{D}^{(i)}$

Measurement domain:

- Total number of measurements: $M = 60$
- Measurement points placed on circles of radius $\rho = 4.5\lambda$

Sources:

- Plane waves
- Number of views: $V = 60$; $\theta_{inc}^{v} = 0^\circ + (v-1) \times (360/V)$
- Amplitude: $A = 1.0$
- Frequency: $F = 300$ MHz ($\lambda = 1$)

Background:

- $\varepsilon_r = 1.0$
- $\sigma = 0$ [S/m]

Scatterer

- Inhomogeneous square object, $\ell = 1.5\lambda$
- $\varepsilon_r^{(1)} \in \{1.02, 1.04, 1.06, 1.08, 1.10, 1.12, 1.14, 1.16, 1.20\}$ (internal circle)
  $\varepsilon_r^{(2)} = \frac{\varepsilon_r^{(1)}}{2}$ (central circle)
  $\varepsilon_r^{(3)} = \frac{\varepsilon_r^{(1)}}{4}$ (external circle)
- $\sigma = 0$ [S/m]

1.1.1 Inhomogeneous Square Object, $\ell = 1.5\lambda$, $\tau^{(1)} = 0.02$ - IMSA-BCS reconstructed profiles

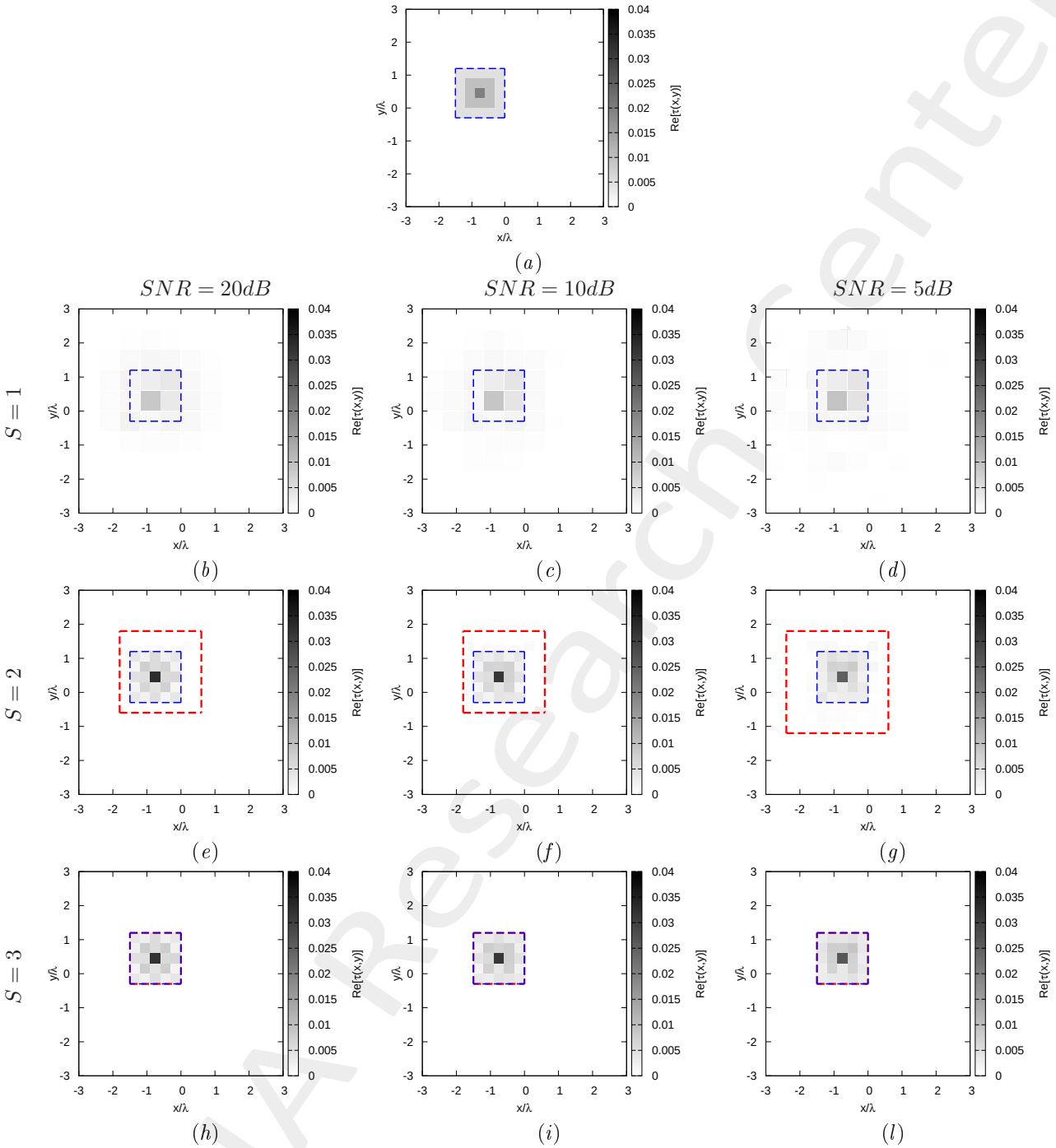

Figure 1: *Inhomogeneous Square Object*, $\ell = 1.5\lambda$, $\tau = 0.02$ - (a) Actual profile and (b)-(o) IMSA-BCS reconstructed profiles for $(b)(e)(h)$ $SNR = 20$ [dB], $(c)(f)(i)$ $SNR = 10$ [dB] and $(d)(g)(l)$ $SNR = 5$ [dB] at the step (b)-(d) $S = 1$, (e)-(g) $S = 2$, and (h)-(l) $S = 3$.

	$SNR = 50dB$			
	$S = 1$	$S = 2$	$S = 3$	$S = 4$
ξ_{tot}	4.01×10^{-4}	1.93×10^{-4}	1.74×10^{-4}	1.74×10^{-4}
ξ_{int}	3.57×10^{-3}	2.95×10^{-3}	2.78×10^{-3}	2.78×10^{-3}
ξ_{ext}	1.89×10^{-4}	9.03×10^{-6}	0.00×10^{-1}	0.00×10^{-1}
	$SNR = 20dB$			
	$S = 1$	$S = 2$	$S = 3$	$S = 4$
ξ_{tot}	4.11×10^{-4}	1.99×10^{-4}	1.72×10^{-4}	1.72×10^{-4}
ξ_{int}	3.64×10^{-3}	3.00×10^{-3}	2.75×10^{-3}	2.75×10^{-3}
ξ_{ext}	1.95×10^{-4}	1.17×10^{-5}	0.00×10^{-1}	0.00×10^{-1}
	$SNR = 10dB$			
	$S = 1$	$S = 2$	$S = 3$	$S = 4$
ξ_{tot}	3.98×10^{-4}	1.98×10^{-4}	1.58×10^{-4}	1.58×10^{-4}
ξ_{int}	3.46×10^{-3}	2.87×10^{-3}	2.53×10^{-3}	2.53×10^{-3}
ξ_{ext}	1.93×10^{-4}	1.98×10^{-5}	0.00×10^{-1}	0.00×10^{-1}
	$SNR = 5dB$			
	$S = 1$	$S = 2$	$S = 3$	$S = 4$
ξ_{tot}	4.15×10^{-4}	2.20×10^{-4}	1.30×10^{-4}	1.30×10^{-4}
ξ_{int}	3.31×10^{-3}	2.76×10^{-3}	2.09×10^{-3}	2.09×10^{-3}
ξ_{ext}	2.18×10^{-4}	5.01×10^{-5}	0.00×10^{-1}	0.00×10^{-1}

Table I: *Inhomogeneous Square Object*, $\ell = 1.5\lambda$, $\tau = 0.02$ - Reconstruction errors: total (ξ_{tot}), internal (ξ_{int}) and external (ξ_{ext}) errors.

	$SNR = 50dB$			
	$S = 1$	$S = 2$	$S = 3$	$S = 4$
$L^{(S)}$	6.00	1.50	1.50	1.50
$N^{(S)}$	100	148	148	148
$Q^{(S)}$	100	64	25	25
	$SNR = 20dB$			
	$S = 1$	$S = 2$	$S = 3$	$S = 4$
$L^{(S)}$	6.00	1.50	1.50	1.50
$N^{(S)}$	100	148	148	148
$Q^{(S)}$	100	64	25	25
	$SNR = 10dB$			
	$S = 1$	$S = 2$	$S = 3$	$S = 4$
$L^{(S)}$	6.00	1.50	1.50	1.50
$N^{(S)}$	100	148	148	148
$Q^{(S)}$	100	64	25	25
	$SNR = 5dB$			
	$S = 1$	$S = 2$	$S = 3$	$S = 4$
$L^{(S)}$	6.00	1.50	1.50	1.50
$N^{(S)}$	100	175	175	175
$Q^{(S)}$	100	100	25	25

Table II: *Inhomogeneous Square Object,* $\ell = 1.5\lambda$, $\tau = 0.02$ - Investigation domain parameters: restricted investigation domain size $L^{(S)}$, total number of cells $N^{(S)}$ and number of cells within the restricted domain size $Q^{(S)}$.

1.1.2 Inhomogeneous Square Object, $\ell = 1.5\lambda$, $\tau^{(1)} = 0.04$ - IMSA-BCS reconstructed profiles

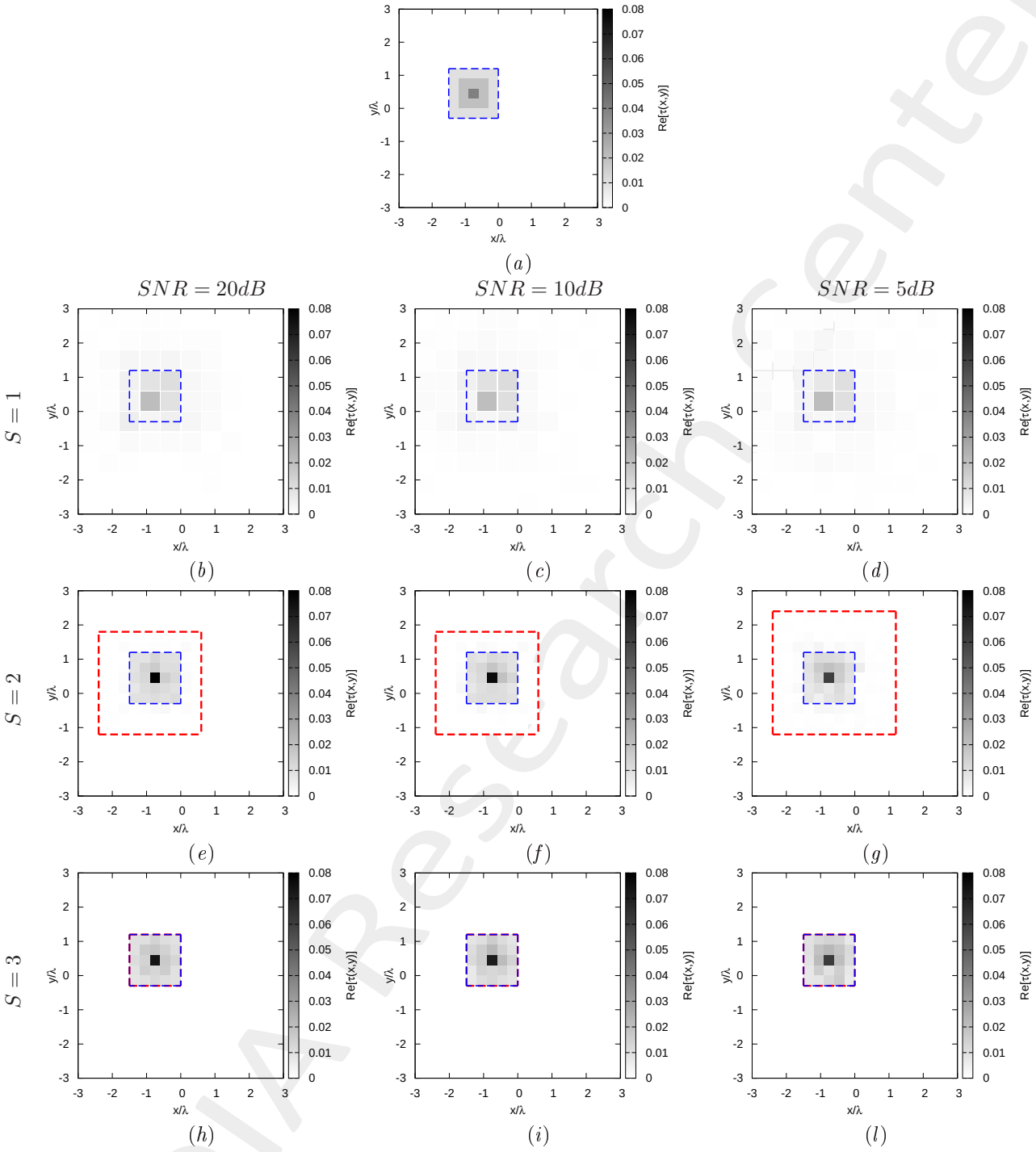

Figure 2: *Inhomogeneous Square Object,* $\ell = 1.5\lambda$, $\tau = 0.04$ - (a) Actual profile and (b)-(o) IMSA-BCS reconstructed profiles for $(b)(e)(h)$ $SNR = 20$ [dB], $(c)(f)(i)$ $SNR = 10$ [dB] and $(d)(g)(l)$ $SNR = 5$ [dB] at the step (b)-(d) $S = 1$, (e)-(g) $S = 2$, and (h)-(l) $S = 3$.

	$SNR = 50dB$			
	$S = 1$	$S = 2$	$S = 3$	$S = 4$
ξ_{tot}	9.35×10^{-4}	3.25×10^{-4}	2.14×10^{-4}	2.14×10^{-4}
ξ_{int}	5.22×10^{-3}	4.44×10^{-3}	3.42×10^{-3}	3.42×10^{-3}
ξ_{ext}	6.39×10^{-4}	5.09×10^{-5}	0.00×10^{-1}	0.00×10^{-1}
	$SNR = 20dB$			
	$S = 1$	$S = 2$	$S = 3$	$S = 4$
ξ_{tot}	9.36×10^{-4}	3.26×10^{-4}	2.13×10^{-4}	2.13×10^{-4}
ξ_{int}	5.15×10^{-3}	4.43×10^{-3}	3.41×10^{-3}	3.41×10^{-3}
ξ_{ext}	6.40×10^{-4}	5.23×10^{-5}	0.00×10^{-1}	0.00×10^{-1}
	$SNR = 10dB$			
	$S = 1$	$S = 2$	$S = 3$	$S = 4$
ξ_{tot}	9.57×10^{-4}	3.19×10^{-4}	4.84×10^{-4}	2.33×10^{-4}
ξ_{int}	5.09×10^{-3}	4.14×10^{-3}	7.75×10^{-3}	3.72×10^{-3}
ξ_{ext}	6.60×10^{-4}	6.18×10^{-5}	0.00×10^{-1}	0.00×10^{-1}
	$SNR = 5dB$			
	$S = 1$	$S = 2$	$S = 3$	$S = 4$
ξ_{tot}	1.08×10^{-3}	4.22×10^{-4}	2.13×10^{-4}	2.13×10^{-4}
ξ_{int}	5.50×10^{-3}	3.93×10^{-3}	3.36×10^{-3}	3.36×10^{-3}
ξ_{ext}	7.56×10^{-4}	1.66×10^{-4}	0.00×10^{-1}	0.00×10^{-1}

Table III: *Inhomogeneous Square Object,* $\ell = 1.5\lambda$, $\tau = 0.04$ - Reconstruction errors: total (ξ_{tot}), internal (ξ_{int}) and external (ξ_{ext}) errors.

	$SNR = 50dB$			
	$S = 1$	$S = 2$	$S = 3$	$S = 4$
$L^{(S)}$	6.00	1.50	1.50	1.50
$N^{(S)}$	100	175	175	175
$Q^{(S)}$	100	100	25	25
	$SNR = 20dB$			
	$S = 1$	$S = 2$	$S = 3$	$S = 4$
$L^{(S)}$	6.00	1.50	1.50	1.50
$N^{(S)}$	100	175	175	175
$Q^{(S)}$	100	100	25	25
	$SNR = 10dB$			
	$S = 1$	$S = 2$	$S = 3$	$S = 4$
$L^{(S)}$	6.00	1.50	1.50	1.50
$N^{(S)}$	100	175	175	175
$Q^{(S)}$	100	100	25	25
	$SNR = 5dB$			
	$S = 1$	$S = 2$	$S = 3$	$S = 4$
$L^{(S)}$	6.00	1.50	1.50	1.50
$N^{(S)}$	100	208	208	208
$Q^{(S)}$	100	144	25	25

Table IV: *Inhomogeneous Square Object*, $\ell = 1.5\lambda$, $\tau = 0.04$ - Investigation domain parameters: restricted investigation domain size $L^{(S)}$, total number of cells $N^{(S)}$ and number of cells within the restricted domain size $Q^{(S)}$.

1.1.3 Inhomogeneous Square Object, $\ell = 1.5\lambda$ - Resume: Errors vs. $\tau^{(1)}$

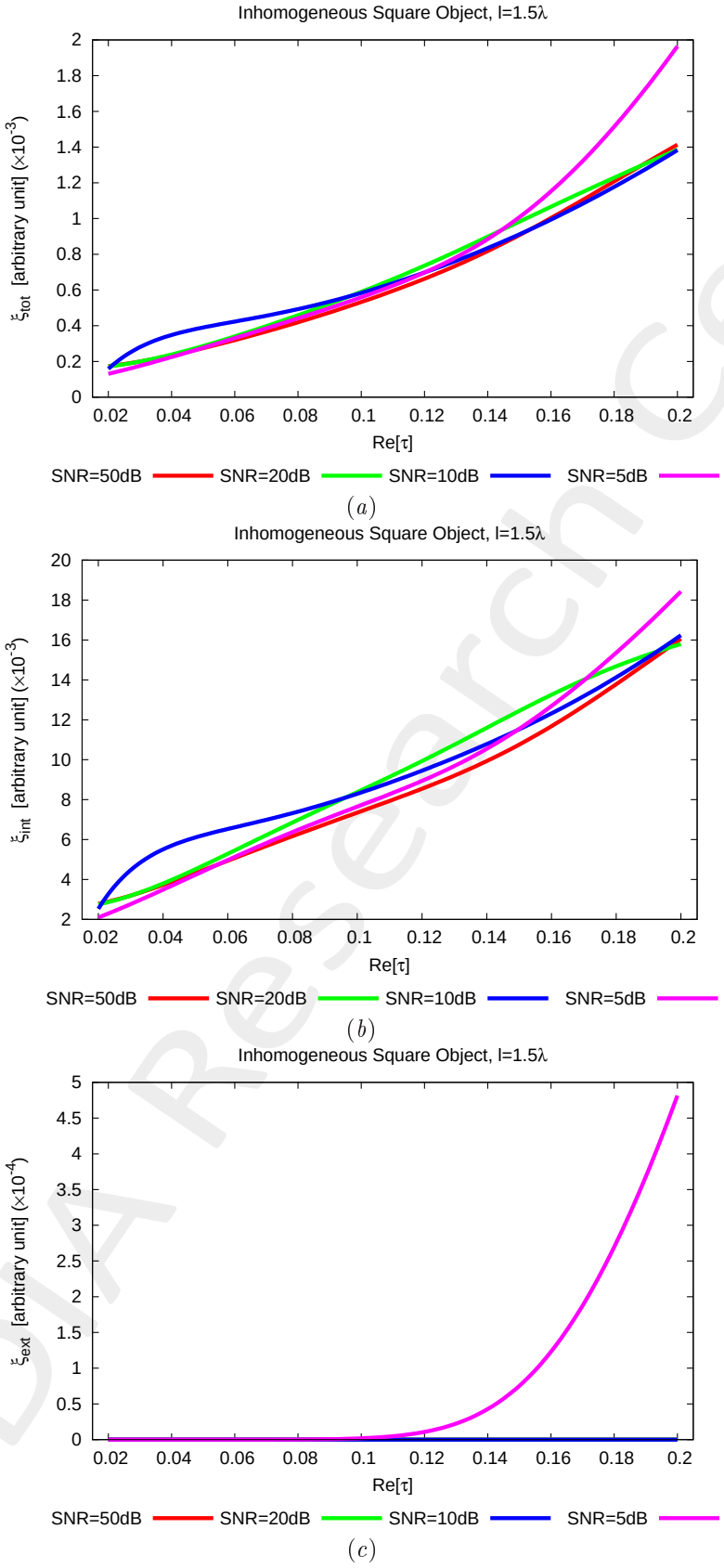

Figure 3: *Inhomogeneous Square Object,* $\ell = 1.5\lambda$ - Reconstruction errors vs. τ: (a) total error, (b) internal error and (c) external error.

1.1.4 Inhomogeneous Square Object, $\ell = 1.5\lambda$ - Resume: Errors vs. SNR

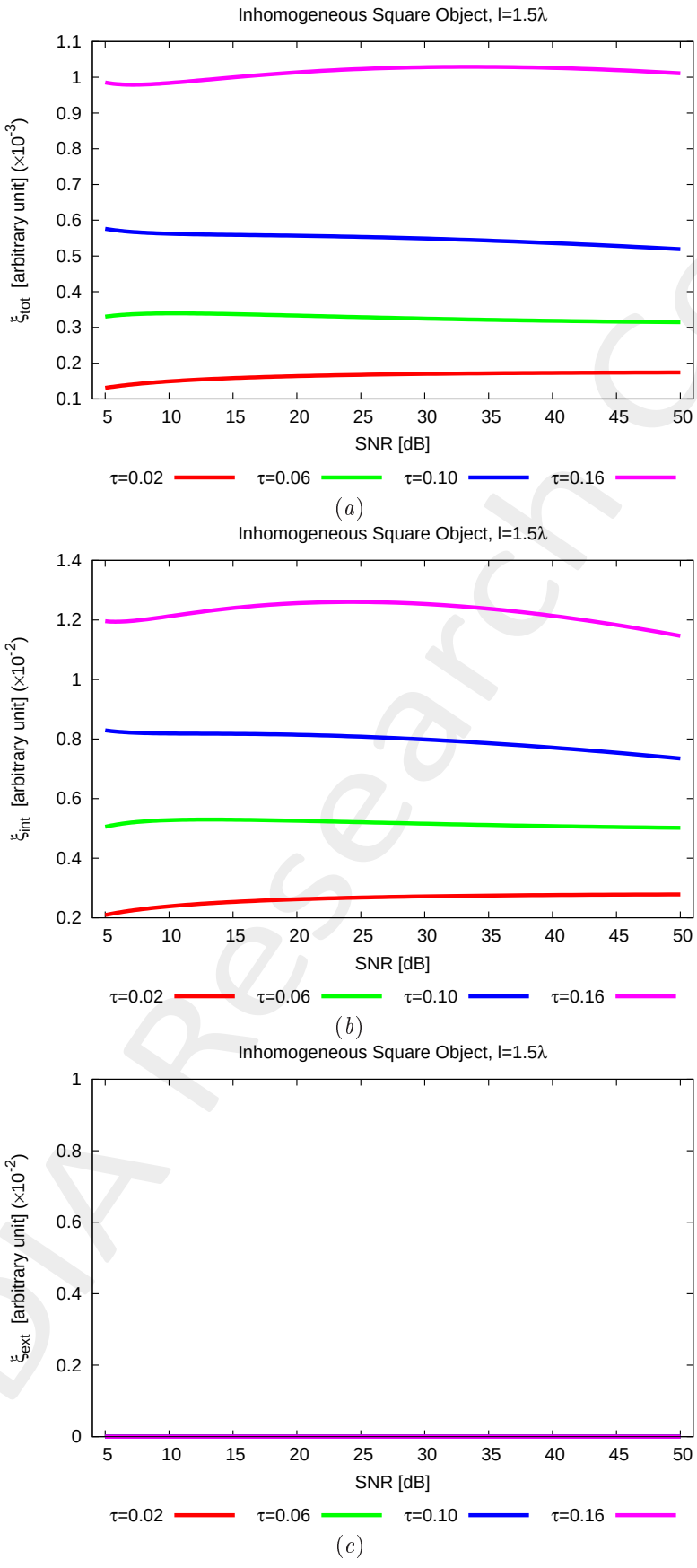

Figure 4: *Inhomogeneous Square Object,* $\ell = 1.5\lambda$ - Reconstruction errors vs. SNR: (a) total error, (b) internal error and (c) external error.

1.1.5 Inhomogeneous Square Object, $\ell = 1.5\lambda$ - Resume: Errors vs. $IMSA$ step, S

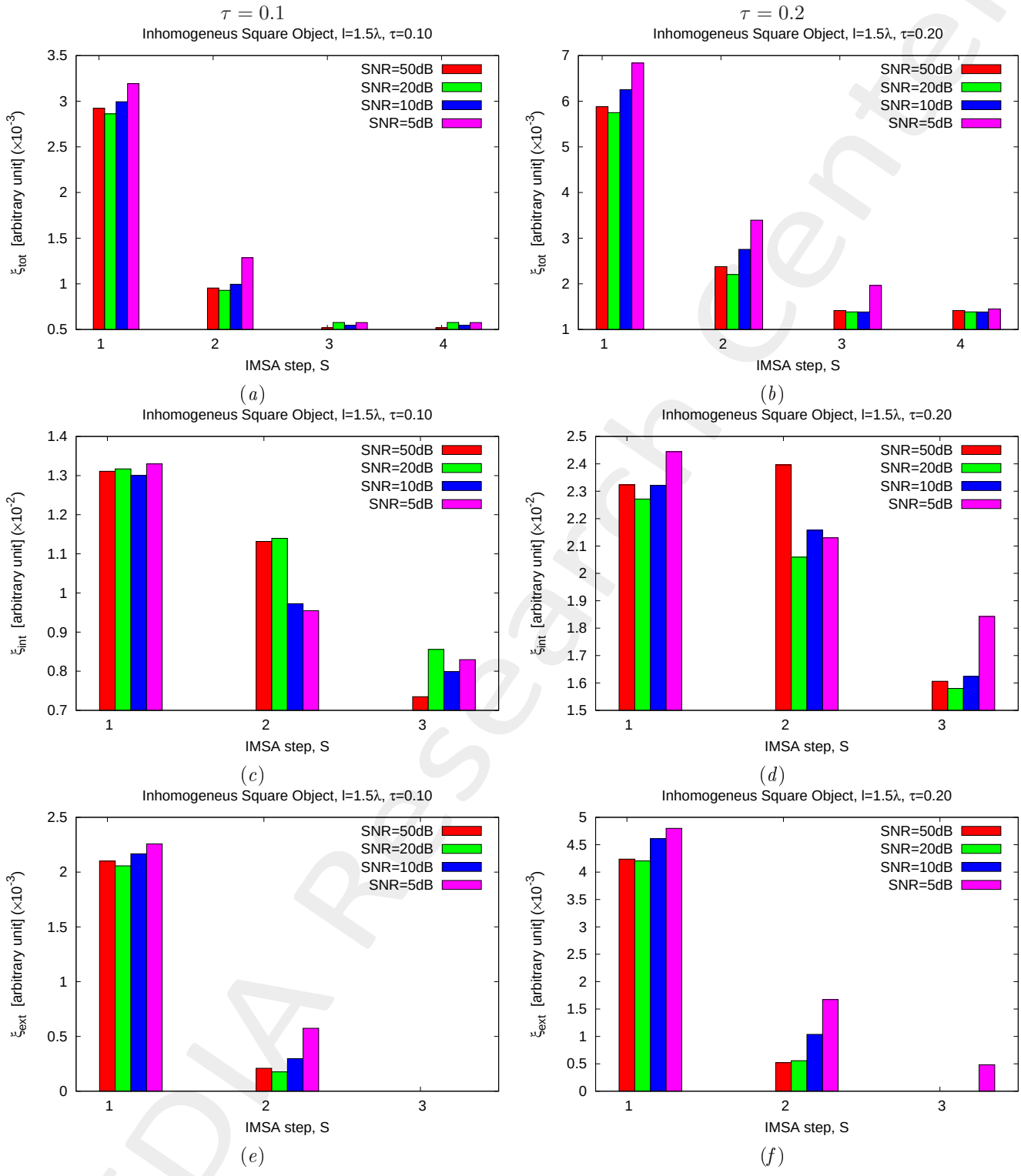

Figure 5: *Inhomogeneous Square Object,* $\ell = 1.5\lambda$ - Reconstruction errors vs. $IMSA$ step, S: $(a)(b)$ total error, $(c)(d)$ internal error and $(e)(f)$ external error for $(a)(c)(e)$ $\tau = 0.1$ and $(b)(d)(f)$ $\tau = 0.2$.

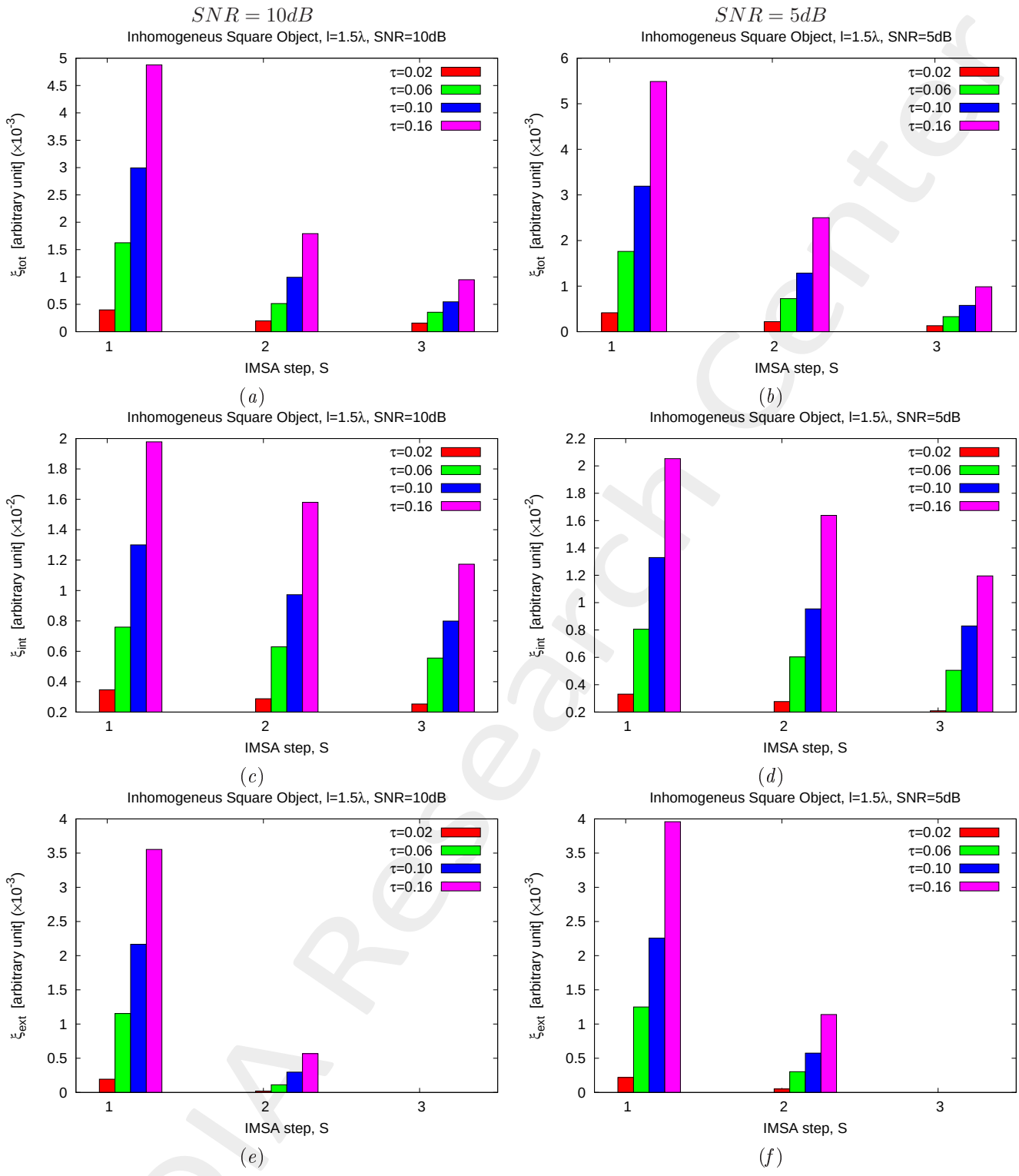

Figure 6: *Inhomogeneous Square Object,* $\ell = 1.5\lambda$ - Reconstruction errors vs. $IMSA$ step, S: $(a)(b)$ total error, $(c)(d)$ internal error and $(e)(f)$ external error for $(a)(c)(e)$ $SNR = 10dB$ and $(b)(d)(f)$ $SNR = 5dB$.

References

[1] M. Salucci, G. Oliveri, and A. Massa, "GPR prospecting through an inverse scattering frequency-hopping multi-focusing approach," *IEEE Trans. Geosci. Remote Sens.*, vol. 53, no. 12, pp. 6573-6592, Dec. 2015.

[2] M. Salucci, L. Poli, N. Anselmi, and A. Massa, "Multifrequency Particle Swarm Optimization for enhanced multiresolution GPR microwave imaging," *IEEE Trans. Geosci. Remote Sens.*, vol. 55, no. 3, pp. 1305-1317, Mar. 2017.

[3] M. Salucci, L. Poli, and A. Massa, "Advanced multi-frequency GPR data processing for non-linear deterministic imaging," *Signal Processing* - Special Issue on 'Advanced Ground-Penetrating Radar Signal-Processing Techniques,' vol. 132, pp. 306-318, Mar. 2017.

[4] N. Anselmi, G. Oliveri, M. Salucci, and A. Massa, "Wavelet-based compressive imaging of sparse targets," *IEEE Trans. Antennas Propag.*, vol. 63, no. 11, pp. 4889-4900, Nov. 2015.

[5] G. Oliveri, M. Salucci, N. Anselmi, and A. Massa, "Compressive sensing as applied to inverse problems for imaging: theory, applications, current trends, and open challenges," *IEEE Antennas Propag. Mag.* - Special Issue on "Electromagnetic Inverse Problems for Sensing and Imaging," vol. 59, no. 5, pp. 34-46, Oct. 2017.

[6] A. Massa, P. Rocca, and G. Oliveri, "Compressive sensing in electromagnetics - A review," *IEEE Antennas Propag. Mag.*, pp. 224-238, vol. 57, no. 1, Feb. 2015.

[7] N. Anselmi, L. Poli, G. Oliveri, and A. Massa, "Iterative multi-resolution bayesian CS for microwave imaging," *IEEE Trans. Antennas Propag.*, vol. 66, no. 7, pp. 3665-3677, Jul. 2018.

[8] N. Anselmi, G. Oliveri, M. A. Hannan, M. Salucci, and A. Massa, "Color compressive sensing imaging of arbitrary-shaped scatterers," *IEEE Trans. Microw. Theory Techn.*, vol. 65, no. 6, pp. 1986-1999, Jun. 2017.

[9] G. Oliveri, N. Anselmi, and A. Massa, "Compressive sensing imaging of non-sparse 2D scatterers by a total-variation approach within the Born approximation," *IEEE Trans. Antennas Propag.*, vol. 62, no. 10, pp. 5157-5170, Oct. 2014.

[10] L. Poli, G. Oliveri, and A. Massa, "Imaging sparse metallic cylinders through a local shape function Bayesian compressive sensing approach," *Journal of Optical Society of America A*, vol. 30, no. 6, pp. 1261-1272, 2013.

[11] L. Poli, G. Oliveri, F. Viani, and A. Massa, "MT-BCS-based microwave imaging approach through minimum-norm current expansion," *IEEE Trans. Antennas Propag.*, vol. 61, no. 9, pp. 4722-4732, Sep. 2013.

[12] F. Viani, L. Poli, G. Oliveri, F. Robol, and A. Massa, "Sparse scatterers imaging through approximated multitask compressive sensing strategies," *Microwave Opt. Technol. Lett.*, vol. 55, no. 7, pp. 1553-1558, Jul. 2013.

[13] L. Poli, G. Oliveri, P. Rocca, and A. Massa, "Bayesian compressive sensing approaches for the reconstruction of two-dimensional sparse scatterers under TE illumination," *IEEE Trans. Geosci. Remote Sens.*, vol. 51, no. 5, pp. 2920-2936, May 2013.

[14] L. Poli, G. Oliveri, and A. Massa, "Microwave imaging within the first-order Born approximation by means of the contrast-field Bayesian compressive sensing," *IEEE Trans. Antennas Propag.*, vol. 60, no. 6, pp. 2865-2879, Jun. 2012.

[15] G. Oliveri, L. Poli, P. Rocca, and A. Massa, "Bayesian compressive optical imaging within the Rytov approximation," *Optics Letters*, vol. 37, no. 10, pp. 1760-1762, 2012.

[16] G. Oliveri, P. Rocca, and A. Massa, "A Bayesian compressive sampling-based inversion for imaging sparse scatterers," *IEEE Trans. Geosci. Remote Sens.*, vol. 49, no. 10, pp. 3993-4006, Oct. 2011.

[17] G. Oliveri, M. Salucci, and N. Anselmi, "Tomographic imaging of sparse low-contrast targets in harsh environments through matrix completion," *IEEE Trans. Microw. Theory Tech.*, vol. 66, no. 6, pp. 2714-2730, Jun. 2018.

[18] M. Salucci, A. Gelmini, L. Poli, G. Oliveri, and A. Massa, "Progressive compressive sensing for exploiting frequency-diversity in GPR imaging," *Journal of Electromagnetic Waves and Applications*, vol. 32, no. 9, pp. 1164- 1193, 2018.